Fluorescence Line-Narrowing Study of Eu^{3+}-Doped Sol−Gel Silica: Effect of Modifying Cations on the Clustering of Eu^{3+}

Vilma C. Costa, Michael J. Lochhead, and Kevin L. Bray*

Department of Chemical Engineering, University of Wisconsin−Madison, Madison, Wisconsin 53706

Received October 16, 1995. Revised Manuscript Received January 2, 1996[⊗]

Fluorescence line-narrowing spectroscopy is used to characterize the effect of metal cation codopants (Sr^{2+}, La^{3+}, Gd^{3+}, Y^{3+}, Lu^{3+}, Sc^{3+}, and Ga^{3+}) on the state of aggregation of Eu^{3+} in sol−gel silica. Significant Eu^{3+} clustering occurs in samples doped only with Eu^{3+}. The addition of codopants inhibits the clustering of Eu^{3+} and promotes better dispersion of Eu^{3+} in the glasses. The extent of the inhibition of clustering increases with field strength of the codopant and levels off at high field strength. The inhibition of clustering is correlated with the generation of strong crystal field bonding sites for Eu^{3+} in the presence of codopants. Characteristics of these sites include the presence of Eu−O−M (M = codopant) linkages and stronger interactions with the network-forming regions of the glass. Supporting luminescence decay and Raman spectroscopy measurements are also presented.

Introduction

In the past decade, many applications of the sol−gel process to the preparation of thin film, fiber, and monolithic optical materials have been reported.[1−5] The potential advantages of the sol−gel method for preparing optical materials include obtaining new chemical compositions, better purity, and more convenient processing conditions. Optical properties achieved in sol−gel materials include[1,2] graded refractive indexes, waveguiding, chemical sensing, optical amplification, frequency doubling, and lasing. In addition to the conventional inorganic sol−gel materials, inorganic−organic hybrid optical materials are currently receiving much attention.[1,2,6,7]

One area of focus has been the preparation of silicate glasses doped with rare-earth or transition-metal ions. Rare earths and transition metals have luminescence properties that make them useful as optical probes of the sol−gel process as well as for luminescence and lasing applications. Eu^{3+} has been most often used as an optical probe because of its particularly informative luminescence spectrum.[8−12] Tb^{3+},[3] Co^{2+},[3,13] Cr^{3+},[14] and $ReCl(CO)_3(bpy)$,[15] and a variety of organic molecules[3,16,17] have also been used as probes. Most of the work on lasing has focused on Nd^{3+} [18,19] or organic dye doping.[20−23] Er^{3+} up-conversion has also been recently reported in sol−gel silica.[24] The optical absorption and/or luminescence properties of several transition-metal and rare-earth ions incorporated into sol−gel silica have been reported, including Cr^{3+},[25,26] Ni^{2+},[27] Fe^{3+},[28] Sm^{2+},[29] Nd^{3+},[30−32] Er^{3+},[33,34] Yb^{3+},[34] and Pr^{3+}.[35] A number of

* Author for correspondence. E-mail: bray@engr.wisc.edu.

[⊗] Abstract published in *Advance ACS Abstracts,* February 15, 1996.

(1) Mackenzie, J. D., Ed. *Sol-Gel Optics III*; SPIE Proceedings Series; SPIE: Bellingham, WA, 1994; Vol. 2288.
(2) Cheetham, A. K., Brinker, C. J., Mecartney, M. L., Sanchez, C., Eds. *Better Ceramics Through Chemistry VI*; Materials Research Symposium Series, Materials Research Society: Pittsburgh, 1994; Vol. 346.
(3) Reisfeld, R.; Jørgensen, C. J. *Struct. Bonding* **1992**, *77*, 207.
(4) Uhlmann, D. R.; Zelinski, B. J. J.; Teowee, G.; Boulton, J. M.; Koussa, A. *J. Non-Cryst. Solids* **1991**, *129*, 76.
(5) Klein, L. C. *Annu. Rev. Mater. Sci.* **1993**, *23*, 437.
(6) Koslova, N. I.; Viana, B.; Sanchez, S. *J. Mater. Chem.* **1993**, *3*, 111.
(7) Sanchez, C., Ribot, F., Eds. *First European Workshop on Hybrid Organic-Inorganic Materials*; Paris, 1993.
(8) Levy, D.; Reisfeld, R.; Avnir, D. *Chem. Phys. Lett.* **1984**, *109*, 593.
(9) McDonagh, C.; Ennis, G.; Marron, P.; O'Kelly, B.; Tang, Z. R.; McGilp, J. F. *J. Non-Cryst. Solids* **1992**, *147* and *148*, 97.
(10) Ferrari, M.; Campostrini, R.; Carturan, G.; Montagna, M. *Philos. Mag. B* **1992**, *65*, 251.
(11) Matthews, L. R.; Wang, X.; Knobbe, E. T. *J. Non-Cryst. Solids* **1994**, *178*, 44.
(12) Lochhead, M. J.; Bray, K. L. *J. Non-Cryst. Solids* **1994**, *170*, 143.
(13) Kojima, K.; Taguchi, H.; Matsuda, J. *J. Phys. Chem.* **1991**, *95*, 7595.
(14) Nie, W.; Boulon, G.; Mai, C.; Esnouf, C.; Xu, R.; Zarzycki, J. *Chem. Mater.* **1992**, *4*, 216.
(15) McKiernan, J.; Pouxviel, J. C.; Dunn, B.; Zink, J. I. *J. Phys. Chem.* **1989**, *93*, 2129.
(16) Dunn, B.; Zink, J. I. *J. Mater. Chem.* **1991**, *1*, 903.
(17) Avnir, D.; Levy, D.; Reisfeld, R. *J. Phys. Chem.* **1984**, *88*, 5956.
(18) Moreshead, W. V.; Nogues, J. R.; Krabill, R. H. *J. Non-Cryst. Solids* **1990**, *121*, 267.
(19) Thomas, I. M.; Payne, S. A.; Wilke, G. D. *J. Non-Cryst. Solids* **1992**, *151*, 183.
(20) Knobbe, E. T.; Dunn, B.; Fuqua, P. D.; Nishida, F. *Appl. Opt.* **1990**, *29*, 2729.
(21) Reisfeld, R.; Seybold, G. *J. Lumin.* **1991**, *48* and *49*, 898.
(22) Salin, F.; Le Saux, G.; Georges, P.; Brun, A.; Bagnall, C.; Zarzycki, J. *Opt. Lett.* **1989**, *14*, 785.
(23) Delmonte, F; Levy, D. *Chem. Mater.* **1995**, *7*, 292.
(24) Xu,W.; Dai, S.; Toth, L. M.; Del Cul, G. D.; Peterson, J. R. *J. Phys. Chem.* **1995**, *99*, 4447.
(25) Tanaka, K.; Kamiya, K. *J. Mater. Sci. Lett.* **1991**, *10*, 1095.
(26) Mass, J. L.; Burlitch, J. M.; Budil, D. E.; Freed, J. H.; Barber, D. B.; Pollock, C. R.; Higuchi, M.; Dieckmann, R. *Chem. Mater.* **1995**, *7*, 1008.
(27) Roy, S.; Ganguli, D. *J. Non-Cryst. Solids* **1992**, *151*, 203.
(28) López, T.; Méndez, J.; Zamudio, T.; Villa, M. *Mater. Chem. Phys.* **1992**, *30*, 161.
(29) Nogami, M.; Abe, Y. *Appl. Phys. Lett.* **1994**, *65*, 1227.
(30) Chakrabarti, S.; Sahu, J.; Chakraborty, M.; Acharya, H. N. *J. Non-Cryst. Solids* **1994**, *180*, 96.
(31) Pope, E. J. A.; Mackenzie, J. D. *J. Am. Ceram. Soc.* **1993**, *76*, 1325.
(32) Fujiyama, T.; Yokoyama, T.; Hori, M.; Sasaki, M. *J. Non-Cryst. Solids* **1991**, *135*, 198.
(33) Wu, F.; Puc, G.; Foy, P.; Snitzer, E.; Sigel, G. H. *Mater. Res. Bull.* **1993**, *28*, 637.

0897-4756/96/2808-0783$12.00/0 © 1996 American Chemical Society

these ions have also been used as dopants in nonsilicate sol−gel matrices.[2,6,36]

Hydroxyl quenching and dopant clustering are two complications that currently limit the luminescence efficiency of rare-earth ions in sol−gel host materials.[19,30,32,37] Hydroxyl quenching is caused by residual water, solvents, and silanol groups present in sol−gel glasses and leads to an enhancement of nonradiative decay pathways of rare-earth ions. Efforts to alleviate hydroxyl quenching have focused on water-removal techniques,[31,38] low hydroxyl syntheses,[39] dopant ion encapsulation,[11] and substitution of hydrophobic groups on the silicon alkoxide precursor.[40] These methods have demonstrated a significant reduction in hydroxyl quenching.

Dopant clustering refers to the tendency of a luminescent species to aggregate with itself through oxygen linkages and is deleterious because it leads to concentration quenching of luminescence through cross-relaxation and energy-transfer processes. The tendency to cluster can also lead to phase separation at the high dopant concentrations normally desired for luminescence and lasing applications.[18,37] Clustering has been detected by electron microscopy in Er^{3+}-[41] and Nd^{3+}-[18]doped sol−gel materials and by lifetime shortening in Nd^{3+}-doped sol−gel materials.[19,31] Rare-earth clustering has been inhibited by codoping with Al^{3+} [18,19,33,42] and by using organic acid salts instead of mineral acid salts as rare-earth precursors.[30] Encapsulation also inhibits clustering but may not be effective at high densification temperatures due to thermal decomposition of the organic encapsulating ligands.

In previous work, we have developed a method for detecting rare-earth clustering in sol−gel glasses based on Eu^{3+} fluorescence line-narrowing spectroscopy.[43] Fluorescence line narrowing (FLN) is a site-selective spectroscopy designed to combat inhomogeneous spectral broadening in glass.[44,45] Inhomogeneous broadening is a consequence of site-to-site variations of the local bonding environment of dopant ions due to the random structural nature of glass. In FLN, a high-resolution laser is used to selectively excite subsets of dopant ions to produce fluorescence spectra characteristic of distinct bonding sites in the glass. By tuning the laser source across an inhomogeneous absorption band, all bonding sites can be sampled. Ideally each excitation energy corresponds to a unique bonding site. In practice, accidental degeneracy can complicate the interpretation of FLN spectra.

To observe a line-narrowing effect (by which we mean the occurrence of fluorescence spectra that vary with excitation energy and exhibit enhanced resolution due to site selectivity and suppression of inhomogeneous broadening) in a glass, it is necessary for the dopant ions to be spatially separated in the glass. If the dopant ions form clusters, the distance between ions will be sufficiently short to permit efficient energy transfer among dopants. As a consequence, dopant ions not selected by the laser become excited, site selectivity is compromised, and an inhomogeneously broadened spectrum is observed. In other words, clustering precludes line narrowing. Using FLN,[43] we were able to demonstrate that clustering occurs in simple Eu^{3+}-doped sol−gel silica, even at low dopant concentrations and that the addition of Al^{3+} as a codopant inhibited the formation of Eu^{3+} clusters.

In this paper we extend our previous work by using FLN spectroscopy to characterize the effect of several cation codopants on the clustering of Eu^{3+} in sol−gel silica. Our goal is to develop an understanding of the codopant properties that promote a uniform distribution of rare-earth ions in sol−gel materials. The codopants considered (Sr^{2+}, La^{3+}, Gd^{3+}, Y^{3+}, Lu^{3+}, Sc^{3+}, and Ga^{3+}) vary in charge and size. The results indicate that the distribution of Eu^{3+} becomes increasingly more uniform with increasing field strength (Z/r^2; Z = ionic charge, r = ionic radius) of the cation codopant.

Experimental Procedure

Sample Preparation. Eu^{3+}-doped silica samples were prepared by combining tetramethoxysilane (TMOS) and an aqueous solution in which $Eu(NO_3)_3 \cdot H_2O$ was previously dissolved. HNO_3 was added to achieve an initial solution pH of 1.5−2. The molar ratio of water to TMOS was 16. Cation codopants were present in the form of nitrate salts ($Sr(NO_3)_2$, $La(NO_3)_3 \cdot 6H_2O$, $Gd(NO_3)_3 \cdot 6H_2O$, $Y(NO_3)_3 \cdot 6H_2O$, $Lu(NO_3)_3 \cdot 6H_2O$, $Sc(NO_3)_3 \cdot 5H_2O$, and $Ga(NO_3)_3 \cdot H_2O$) in the aqueous europium nitrate solution. The aqueous solution was mixed under vigorous stirring with TMOS. The europium salt concentration is expressed in terms of the weight percent of Eu_2O_3 that would be present in a hypothetical, fully densified SiO_2 glass free of residual water and organics. All samples contained 1 wt % Eu_2O_3. The codopant concentration was varied to give 3:1 and 9:1 molar ratios of codopant to Eu^{3+}.

After homogenization, these sols were cast into plastic containers where they were allowed to gel at room temperature. Gel times varied from 2 to 5 days depending on the codopant concentration and the volume of solution that was cast in the containers. After gelation the samples were aged at 60 °C for 2 days and dried at 90 °C for 2 days. Further heat treatment in air was carried out in a box furnace. The samples discussed in this work were heated to 800 °C. Transparent monolithic solid samples were obtained for all codopant concentrations. No visual evidence of phase separation was observed.

Spectroscopic Measurements. The broad-band emission spectra were obtained using a tungsten−halogen lamp equipped with a dielectric filter passing all wavelengths shorter than 500 nm. Luminescence was collected and focused on a 1- m monochromator and detected by a photomultiplier tube (PMT). All broad-band spectra were collected at room temperature.

In the fluorescence line-narrowing measurements, a high-resolution pulsed tunable dye laser pumped by a Q-switched

(34) Moutonnet, D.; Chaplain, R.; Gauneau, M.; Pelous, Y.; Rehspringer, J. L. *Mater Sci. Eng.* **1991**, *B9*, 455.
(35) Sun, K.; Lee, W.; Risen, W. M. *J. Non-Cryst. Solids* **1987**, *92*, 145.
(36) Bahtat, A.; Bouazoui, M.; Bahtat, M.; Mugnier, J. *Opt. Commun.* **1994**, *111*, 55.
(37) Pope, E. J. A.; Mackenzie, J. D. *J. Non-Cryst. Solids* **1988**, *106*, 236.
(38) Brinker, C. J.; Scherer, G. W. *Sol-Gel Science*; Academic Press: Boston, 1990.
(39) Yuh, S.; Bescher, E. P.; Babonneau, F.; Mackenzie, J. D. In *Better Ceramics Through Chemistry VI*; Materials Research Symposium Series; Cheetham, A. K., Brinker, C. J., Mecartney, M. L., Sanchez, C., Eds; Materials Research Society: Pittsburgh, 1994; Vol. 346, p 803.
(40) Sanchez, C.; Lebeau, B.; Viana, B. In *Sol-Gel Optics III*; SPIE Proceedings Series; Mackenzie, J. D., Ed.; SPIE: Bellingham, WA, 1994; Vol. 2288, p 227.
(41) Lee, L.; Tsai, D. *J. Mater. Sci. Lett.* **1994**, *13*, 615.
(42) Fujiyama, T.; Hori, M.; Sasaki, M. *J. Non-Cryst. Solids* **1990**, *121*, 273.
(43) Lochhead, M. J.; Bray, K. L. *Chem. Mater.* **1995**, *7*, 572.
(44) Yen, W. M. In *Optical Spectroscopy of Glasses*; Zschokke, I., Ed.; D. Reidel Publishing Co.: Dordrecht, The Netherlands, 1986; pp 23−64.
(45) Weber, M. J. In *Laser Spectroscopy of Solids*, Topics in Applied Physics; Springer-Verlag: Berlin, 1981; Vol. 49, pp 189−239.

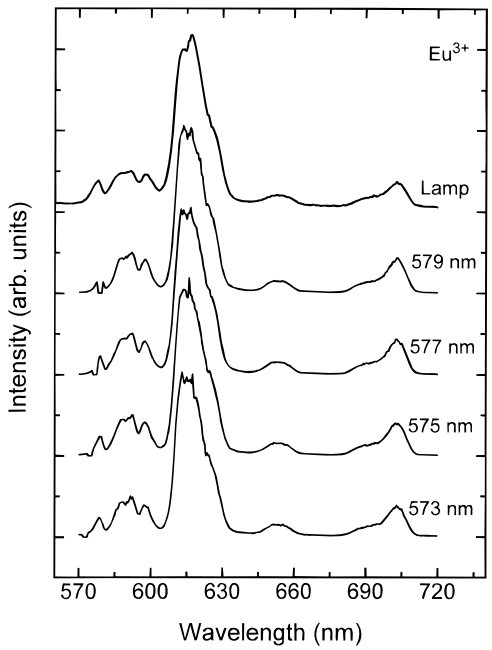

Figure 1. Emission spectra (77 K) of 1 wt % Eu_2O_3-doped sol−gel silica at various excitation wavelengths. Intensities were normalized to the $^5D_0 \rightarrow {}^7F_1$ emission at each pump wavelength. Upper spectrum, fluorescence spectrum at 300 K excited with a tungsten lamp, $\lambda_{ex} \leq 500$ nm.

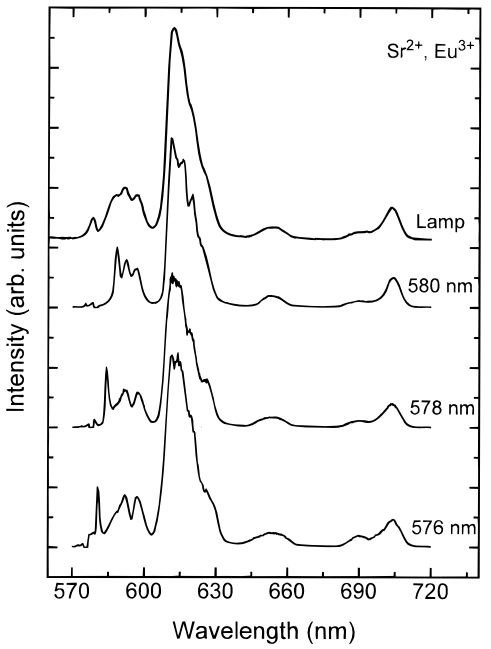

Figure 2. FLN spectra at 77 K of 1 wt % Eu_2O_3-doped sol−gel silica codoped with Sr^{2+} (molar ratio $Sr^{2+}/Eu^{3+} = 9$) at various excitation wavelengths. Intensities were normalized to the $^5D_0 \rightarrow {}^7F_1$ emission at each pump wavelength. Upper spectrum, fluorescence spectrum at 300 K excited with a tungsten lamp, $\lambda_{ex} \leq 500$ nm.

Nd:YAG laser was used as the excitation source. The dye laser pulse duration was approximately 10 ns with a laser linewidth of 0.1 cm^{-1}. The dye laser provided the tunable emission from 573 to 580 nm needed to selectively excite the $^7F_0 \rightarrow {}^5D_0$ transition of Eu^{3+}. Samples were mounted in a liquid nitrogen optical cryostat. Emission from Eu^{3+} was passed through a 1-m monochromator and detected by a PMT. Spectra are normalized to the $^5D_0 \rightarrow {}^7F_1$ peak intensity. For the luminescence decay measurements, the signal detected by the PMT was recorded by a digital storage oscilloscope.

Raman spectra were collected in backscattering geometry using the 488 nm line of an argon laser in conjunction with a double monochromator and single-photon counting techniques. Experimental conditions included 5 cm^{-1} resolution and a 5 s counting time per data point.

Results

Fluorescence Line-Narrowing Measurements. *Eu*$^{3+}$*-Doped Sol−Gel Silica.* Figure 1 shows the fluorescence line-narrowing spectra of 1 wt % Eu_2O_3-doped sample of sol−gel silica densified at 800 °C. The spectra were obtained by selective excitation across the inhomogeneously broadened $^7F_0 \rightarrow {}^5D_0$ absorption band with the dye laser tuned at 1 nm intervals. The upper trace shows the conventional broad band luminescence spectrum of Eu^{3+}. The broad-band spectrum is comprised of contributions from all Eu^{3+} bonding sites. The spectrum consists of transitions from the $^5D_0$ level of Eu^{3+} to the $^7F_0$ (single band near 578 nm), $^7F_1$ (bands between ~582 and 605 nm), $^7F_2$ (intense band between ~610 and 630 nm), $^7F_3$ (weak band near 655 nm), and $^7F_4$ (bands between ~690 and 710 nm) levels. No emission from levels above $^5D_0$ was observed. The lower traces show Eu^{3+} luminescence spectra after selective excitation at the wavelengths indicated in the figure. The flat response centered about the excitation wavelength in each spectrum corresponds to wavelengths that were intentionally blocked to prevent exposure of the detector to direct laser light.

The most noteworthy feature of Figure 1 is the insensitivity of the spectra to excitation wavelength. The spectra for the individual wavelengths were similar to the broad-band result and no fluorescence line-narrowing effect was observed. On the basis of a previous study of Eu^{3+}-doped densified sol−gel silica derived from TEOS,[43] we attribute the lack of line narrowing to the clustering of Eu^{3+}. Clustering of Eu^{3+} leads to short $Eu^{3+}-Eu^{3+}$ distances, efficient energy transfer between adjacent Eu^{3+} ions and a loss of site selectivity. In addition to the lack of line narrowing, the presence of $^5D_0 \rightarrow {}^7F_0$ emission intensity adjacent to the range of blocked wavelengths was an indication of energy transfer. The emission arises from Eu^{3+} ions that were not excited directly by the laser and will be referred to as nonselective emission in this paper.

Eu^{3+}*-Doped Sol−Gel Silica Codoped with Sr*$^{2+}$. Figure 2 shows broad-band and selectively excited emission spectra for 1 wt % Eu_2O_3 silica gel codoped with strontium (molar ratio $Sr^{2+}:Eu^{3+} = 9$). In contrast to the Eu^{3+}-only-doped system, the Sr^{2+} codoped system exhibited a line-narrowing effect. The effect was most notable in the $^5D_0 \rightarrow {}^7F_1$ transition where the position of the high-energy component depended significantly on the excitation wavelength. A similar sensitivity of this spectral component to excitation wavelength is commonly observed in Eu^{3+}-doped melt glasses.[46,47] Less significant variations in the $^5D_0 \rightarrow {}^7F_2$, $^7F_3$, $^7F_4$ transitions were observed with excitation wavelength. Note also that the nonselective $^5D_0 \rightarrow {}^7F_0$ fluorescence intensity was weaker in the presence of the Sr^{2+} codopant.

Eu^{3+}*-Doped Sol−Gel Silica Codoped with Gd*$^{3+}$. Figure 3 shows the broad-band and line-narrowed emission

(46) Brecher, C.; Riseberg, L. A. *Phys. Rev. B* **1976**, *13*, 81.
(47) Belliveau, T. F.; Simkin, D. J. *J. Non-Cryst. Solids* **1989**, *110*, 127.

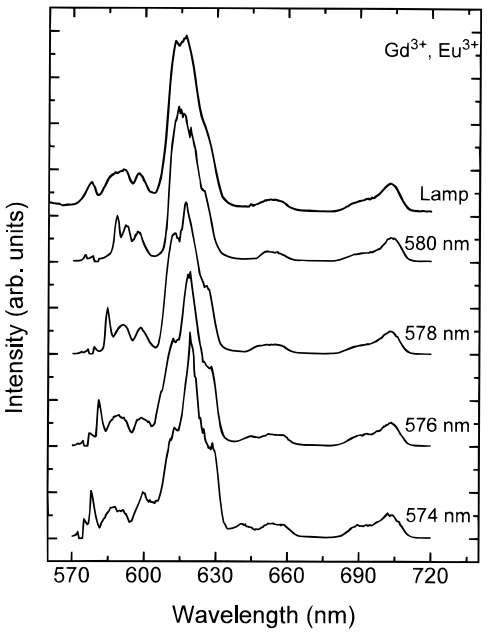

Figure 3. FLN spectra at 77 K of 1 wt % Eu_2O_3-doped sol−gel silica codoped with Gd^{3+} (molar ratio $Gd^{3+}/Eu^{3+} = 9$) at various excitation wavelengths. Intensities were normalized to the $^5D_0 \rightarrow {}^7F_1$ emission at each pump wavelength. Upper spectrum, fluorescence spectrum at 300 K excited with a tungsten lamp, $\lambda_{ex} \leq 500$ nm.

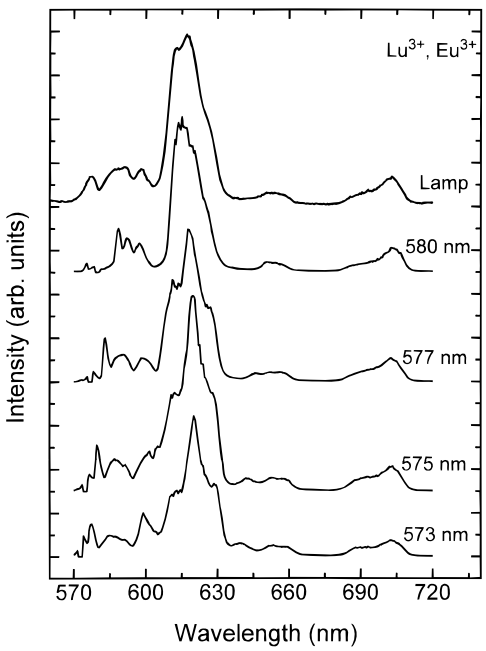

Figure 4. FLN spectra at 77 K of 1 wt % Eu_2O_3-doped sol−gel silica codoped with Lu^{3+} (molar ratio $Lu^{3+}/Eu^{3+} = 9$) at various excitation wavelengths. Intensities were normalized to the $^5D_0 \rightarrow {}^7F_1$ emission at each pump wavelength. Upper spectrum, fluorescence spectrum at 300 K excited with a tungsten lamp, $\lambda_{ex} \leq 500$ nm.

spectra for 1 wt % Eu_2O_3 silica codoped with a 9:1 molar ratio of Gd^{3+}:Eu^{3+}. Line-narrowing effects were again evident and were more pronounced than in the case of Sr^{2+} codoping. The broad-band spectral features appeared to be broader as well, a result that indicates the presence of a wider range of bonding environments for Eu^{3+}. As in the case of Sr^{2+} codoping, a significant variation of the $^5D_0 \rightarrow {}^7F_1$ transition was observed with excitation wavelength. In addition, more pronounced changes in the other transitions were observed in the presence of Gd^{3+}. A decrease in the excitation wavelength led to an intensity reduction of the short-wavelength side of the $^5D_0 \rightarrow {}^7F_2$ transition and a splitting of the $^5D_0 \rightarrow F_3$ transition.

Eu^{3+}-Doped Sol−Gel Silica Codoped with Lu^{3+}. The FLN spectra at 77 K for a 1 wt % Eu_2O_3 silica gel with a 9:1 molar ratio of Lu^{3+}:Eu^{3+} are shown in Figure 4. The changes of the FLN spectra upon codoping with Lu^{3+} appeared to be a continuation of the trends seen for the Sr^{2+} and Gd^{3+} codopants. The line-narrowing effect was clearly evident and significant spectral changes were observed. Relative to the Gd^{3+} codoped sample, a more pronounced decrease in the short-wavelength $^5D_0 \rightarrow {}^7F_2$ intensity and further splitting of the $^5D_0 \rightarrow {}^7F_3$ transition were observed. The relative intensity of the two broad features associated with the $^5D_0 \rightarrow {}^7F_4$ transition also exhibited a greater dependence on excitation wavelength.

Eu^{3+}-Doped Sol−Gel Silica Codoped with Other Cations. In addition to the samples discussed above, we also considered samples containing the codopants La^{3+}, Y^{3+}, Sc^{3+}, and Ga^{3+} in a 9:1 molar ratio with Eu^{3+}. The spectral changes observed in the FLN spectra of these samples were qualitatively similar to the changes described above. The sensitivity of spectral changes to excitation wavelength was a function of the codopant and varied for the cations of this study according to $Sr^{2+} < La^{3+} < Gd^{3+} < Y^{3+} < Lu^{3+} \sim Sc^{3+} \sim Ga^{3+}$. We also considered samples with the codopants in a 3:1 molar ratio with Eu^{3+}. Line-narrowing effects were observed for these samples but were less pronounced than in the 9:1 samples. The same trend in spectral sensitivity with respect to excitation wavelength was observed for the 3:1 and 9:1 samples.

Decay Measurements. Fluorescence decay curves at 77 K for the $^5D_0$ level were obtained at excitation wavelengths of 577 and 579 nm for all of the samples. Decay curves were measured at emission wavelengths of 610 and 625 nm for both excitation wavelengths. Selected results are shown in Figure 5. The decay curves of the sample containing only Eu^{3+} were nearly pure exponentials with a lifetime of 1.23 ms that was independent of the excitation and detection wavelengths to within the accuracy of our measurements (±0.05 ms).

The decay curves of the codoped samples were slightly nonexponential and appeared to consist of a fast-decay component and a slow-decay component. Since double-exponential fits can be ambiguous and are not needed for the purposes of this paper, we decided to report an average lifetime defined as the area under the normalized decay curve[48] for each sample. For a pure exponential decay, the average lifetime defined in this way is equal to the time constant of the decay. The average lifetimes are listed for the 9:1 samples in Table 1 for the different excitation and emission wavelengths.

The lifetimes for the codoped samples were considerably longer than the lifetime for the samples doped only with Eu^{3+}. To our knowledge, the lifetime of the Sr^{2+} codoped glass (~2.4 ms) is the longest ever reported for Eu^{3+} in a sol−gel glass. For comparison purposes, Eu^{3+} lifetimes in melt prepared silicate glasses are typically 1−2 ms.[46]

(48) Armagan, G.; Buoncristiani, A. M.; DiBartolo, B. *J. Lumin.* **1989**, *44*, 129.

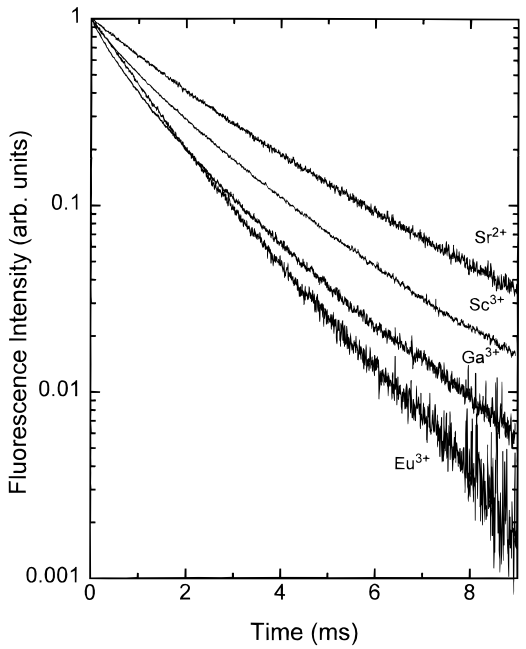

Figure 5. Normalized decay curves of the Eu^{3+}-doped and selected codoped samples. The excitation and monitoring wavelengths are 577 and 610 nm, respectively, for each decay curve.

Table 1. Lifetime Values (±0.05 ms) Measured at 77 K for 1 wt % Eu_2O_3 Sol−Gel Silica Glasses Codoped with Various Cations[a]

	λ_{mon} (nm)			
	λ_{exc} = 577 nm		λ_{exc} = 579 nm	
	610	625	610	625
Sr^{2+}	2.42	2.26	2.48	2.50
La^{3+}	1.81	1.60	1.88	1.77
Gd^{3+}	1.81	1.55	1.82	1.67
Y^{3+}	1.67	1.49	1.74	1.59
Lu^{3+}	1.75	1.52	1.85	1.69
Sc^{3+}	1.68	1.52	1.75	1.64
Ga^{3+}	1.26	1.17	1.34	1.33

[a] The lifetimes were obtained from the area under normalized decay curves, as discussed in the text. Lifetime values were measured for two excitation wavelengths (577, 579 nm) and two monitoring wavelengths (610, 625 nm).

Discussion

The incorporation of rare-earth ions into melt prepared silicate glasses is problematic because of the tendency for phase separation to occur due to the low solubility of rare-earth oxides in silica.[18,19,31,42] The sol−gel process represents an alternative route to rare-earth-doped glass and offers the potential to achieve the higher doping concentrations desired for many applications. To realize this potential, however, it is necessary to prepare sol−gel glasses with a spatially uniform distribution of rare-earth dopants. Recent work has demonstrated the tendency of rare-earth (and other metal) ions to form clusters in sol−gel silica.[6,18,19,41] Further understanding of the factors that govern metal-ion clustering is needed in order to constructively control the spatial distribution of dopants in sol−gel glasses.

Effect of Codopants on Eu^{3+} Clustering. We have recently proposed a method based on Eu^{3+} fluorescence line-narrowing spectroscopy for qualitatively detecting clustering in sol−gel silica and have shown that Eu^{3+} clustering is significant even at low dopant concentration.[43] The spectra of the sample doped only with Eu^{3+} shown in Figure 1 illustrate a situation where significant clustering is expected to be present. The selective excitation spectra show little or no variation with excitation wavelength and strongly resemble the broad-band result. The absence of line narrowing is consistent with clustering because the short Eu^{3+}−Eu^{3+} distances associated with clustering lead to efficient energy transfer among Eu^{3+} ions. Energy transfer provides a mechanism for exciting Eu^{3+} ions not directly excited by the laser, and as a consequence a spectrum similar to the broad-band one results.

Table 2. Ionic Radii, Charge Densities, and Field Strengths of the Codopants Used in This Study[a]

cation	ion radius, r (Å)	charge density, Z/r ($Å^{-1}$)	field strength, Z/r^2 ($Å^{-2}$)
Sr^{2+}	1.160	1.724	1.486
La^{3+}	1.061	2.828	2.665
Eu^{3+}	0.950	3.158	3.324
Gd^{3+}	0.938	3.198	3.410
Y^{3+}	0.892	3.363	3.770
Lu^{3+}	0.848	3.538	4.172
Sc^{3+}	0.730	4.110	5.630
Ga^{3+}	0.620	4.839	7.804

[a] The ionic radii correspond to 6-fold coordination in an oxide environment (Shannon, R. D.; Prewitt, C. T. *Acta Crystallogr.* **1969**, *B25*, 925).

Figures 2−4 and similar data not shown for the other codopants clearly indicate that the presence of a cation codopant has a strong influence on the local bonding environment of Eu^{3+}. All the codopants lead to the development of a line-narrowing effect. We attribute the effect to the ability of the codopants to penetrate Eu^{3+} clusters or to inhibit their formation. In either case, the average Eu^{3+}−Eu^{3+} distance increases. As a result, energy transfer decreases and site selectivity is observed.

Quantitatively, the degree of site selectivity varies with the cation codopant. The most pronounced spectral variations with excitation wavelength were observed for Lu^{3+}, Sc^{3+}, and Ga^{3+}. Increasingly less pronounced variations were observed for Y^{3+}, Gd^{3+}, La^{3+}, and Sr^{2+}. These observations suggest that the ability of the codopants to inhibit Eu^{3+} clustering decreases as Ga^{3+} ~Sc^{3+} ~Lu^{3+} > Y^{3+} > Gd^{3+} > La^{3+} > Sr^{2+}. This ordering is significant because it parallels the trend observed for the field strength (Z/r^2) (or charge density (Z/r)) of the cation codopants (Table 2). We therefore propose that high field strength cation codopants are more effective at inhibiting Eu^{3+} clustering and promoting a more uniform distribution of Eu^{3+} ions than low field strength codopants.

The similarity of the spectra for the samples codoped with Lu^{3+}, Sc^{3+}, and Ga^{3+} implies that the effect of field strength saturates beyond a certain value or that the FLN technique is not sensitive enough to discern the differences. The latter possibility seems unlikely in light of our previous study[43] of TEOS (tetraethoxysilane) based glasses doped with Al^{3+} (field strength = 11.53 $Å^{-2}$) and Eu^{3+} in a 10:1 molar ratio which showed line-narrowing effects that were more pronounced than those observed for Lu^{3+}, Sc^{3+}, and Ga^{3+} in this study. The comparison with Al^{3+} is complicated by the fact, however, that Al^{3+} will act as a network former, whereas Lu^{3+}, Sc^{3+}, and Ga^{3+} are expected to act as network modifiers. It is possible that the charge density effect

saturates for modifiers and that the network-forming capability rather than the charge density governs the effect of Al^{3+} on the clustering of Eu^{3+}. It is also possible that smaller concentrations of high-charge-density modifiers are as effective at inhibiting Eu^{3+} clustering as larger concentrations of low-charge-density modifiers. A comparison of our 3:1 and 9:1 molar ratio samples provides tentative support for this possibility. Further work is needed to clarify these points.

Local Bonding Environment of Eu^{3+}. The results of this study support the modified random network model of glass structure proposed by Greaves.[49] This model proposes that modifying cations are not distributed randomly in glass but rather that they have a tendency to aggregate locally with some degree of ordering. The overall structure of the glass is proposed to consist of randomly distributed modifier-rich and modifier-deficient domains. The modifier-rich regions are largely ionic, while the modifier-deficient regions are largely covalent and comprised predominantly of network-forming species.

This picture is consistent with the spectral results obtained for the sample doped only with Eu^{3+}. The clustering inferred from the selective excitation measurements of the sample (Figure 1) is consistent with the presence of Eu^{3+}-rich regions in which short Eu^{3+}–Eu^{3+} distances are present. The lack of visually observable phase separation suggests that the clustering occurs locally and that distinct, isolated clusters are distributed throughout the glass. Inhomogeneous broadening occurs because of disorder within the clusters (which will likely vary with the cluster) and differences in the interaction of individual clusters with the network-former-rich regions of the glass.

When a cation codopant is present, the crystal chemistry interpretation[50] of the modified random network model is supported by our results. According to the crystal chemistry approach, multiple cation modifiers will coexist in the modifier-rich regions and will be randomly mixed within these regions. This implies that when a codopant is added to an Eu^{3+}-doped sample, it will penetrate the Eu^{3+} clusters and promote interdispersion. The interdispersion occurs because of the formation of Eu–O–M linkages, where M is a codopant. The net effect is an increased separation and reduced energy transfer between Eu^{3+} ions. This argument is consistent with the development of a line-narrowing effect in the codoped samples (Figures 2–4).

Evidence for the formation of the Eu–O–M linkages can be found by examining the $^5D_0 \rightarrow {}^7F_0$ fluorescence of Eu^{3+}. The $^5D_0 \rightarrow {}^7F_0$ transition is an effective diagnostic of the bonding environment of Eu^{3+} because it does not exhibit a crystal field splitting and its energy provides information on the covalency of Eu^{3+} bonding.[51,52] (Note that crystal field strength is a quantity distinct from the field strength of a codopant. The former is a property of the bonding site of Eu^{3+} and in simplest terms is describable in terms of point charge interactions between Eu^{3+} and its nearest neighbors. The latter is a property only of a codopant ion and has been defined in Table 2. To avoid confusion, crystal field strength and field strength will be used to refer to the former and latter quantities, respectively.) The energy of the $^5D_0 \rightarrow {}^7F_0$ transition is a consequence of the nephelauxetic effect, and there is a general tendency to observe lower energies for the transition in more covalent bonding environments and higher energies when the bonding is more ionic.

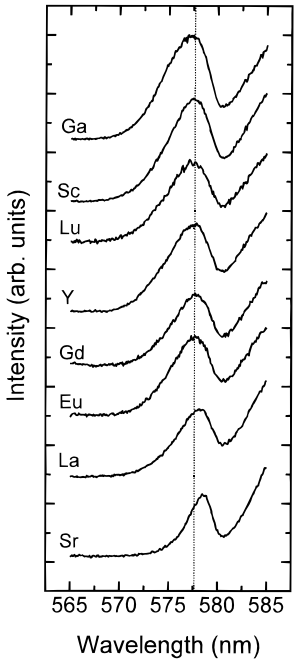

Figure 6. Room-temperature $^5D_0 \rightarrow {}^7F_0$ fluorescence spectra (tungsten lamp) of 1 wt % Eu_2O_3-doped sol–gel silica with various codopants (molar ratio codopant/Eu^{3+} = 9). All spectra are normalized to the peak intensity.

The field strength of the codopant will influence the covalency of the Eu–O bond.[53,54] Higher field strength codopants M in linkages will form stronger, more covalent bonds with oxygen. This in turn leads to weaker, less covalent Eu–O bonds in the linkage. In effect, there is a competition between Eu^{3+} and the codopant for the electron density associated with oxygen and the higher field strength cation exerts the controlling influence. As a result, we expect the $^5D_0 \rightarrow {}^7F_0$ transition to occur at increasingly shorter wavelengths as the codopant field strength increases.

Figure 6 summarizes the effect of cation codopant on the $^5D_0 \rightarrow {}^7F_0$ transition for the 9:1 molar ratio samples. The spectra from bottom to top in the figure are presented in the order of increasing codopant field strength (or charge density). The spectrum for the sample doped only with Eu^{3+} serves as a useful reference. The main effect observed in Figure 6 is a general broadening on the short-wavelength side of the transition as the codopant field strength increases. Since the $^5D_0 \rightarrow {}^7F_0$ transition is nondegenerate, a larger bandwidth indicates that a wider range of bonding environments is present for Eu^{3+}. Increased short-wavelength broadening is consistent with the generation of new bonding sites for Eu^{3+} which include Eu–O–M linkages.

The FLN spectra shown in Figures 2–4 provide additional information about the new sites. Short-

(49) Greaves, G. N. *J. Non-Cryst. Solids* **1985**, *71*, 203.
(50) Wang, J.; Brocklesby, W. S.; Lincoln, J. R.; Townsend, J. E.; Payne, D. N. *J. Non-Cryst. Solids* **1993**, *163*, 261.
(51) Albin, M.; Horrocks, W. D. *Inorg. Chem.* **1985**, *24*, 895.
(52) Caro, P.; Beaury, O.; Antic, E. *J. Phys.* **1976**, *37*, 671.
(53) Ellison, A. J. G.; Hess, P. C. *J. Non-Cryst. Solids* **1991**, *127*, 247.
(54) Ellison, A. J. G.; Hess, P. C. *J. Geophys. Res.* **1990**, *B95*, 15717.

wavelength excitation will lead to selective excitation of the new sites, and the resulting FLN spectra will be characteristic of the bonding environments of those sites. Regardless of the codopant, the main effect observed with decreasing excitation wavelength was increased splitting of the fluorescence transitions. This effect is particularly evident for the $^5D_0 \rightarrow {}^7F_1$ transition. The larger splittings associated with short excitation wavelengths indicate that the new Eu^{3+} sites created upon codoping are strong crystal field sites.[55−57] A decrease in the intensity of the short-wavelength side of the $^5D_0 \rightarrow {}^7F_2$ transition was also consistently observed in the codoped samples as the excitation wavelength was decreased.

The FLN spectra also reveal significant differences in the effect of the different codopants on the local bonding environment of Eu^{3+} and indicate that more pronounced effects are associated with higher field strength codopants. The correlation to codopant field strength suggests a relationship between the spectral results and the state of polymerization of the silica framework of the glass. One way to assess the state of polymerization is to determine the relative concentrations of silicon Q^n species. In Q^n notation, *n* refers to the number of bridging oxygens bonded to silicon. Thus, a Q^4 species corresponds to a fully polymerized silicon atom and a Q^0 species refers to an unpolymerized orthosilicate unit.

Raman studies of melt prepared silica glass modified by alkali,[58,59] alkaline earth,[60,61] and rare-earth[53,54] ions have shown that high field strength modifiers favor the disproportionation of Q^n species through reactions such as

$$2Q^3 \leftrightarrow Q^4 + Q^2$$

$$2Q^2 \leftrightarrow Q^3 + Q^1$$

Since each Q^n species has a characteristic Raman band associated with it, changes in the relative intensities of Raman features provide a measure of the effect of modifier field strength on the state of polymerization of a glass.

Raman scattering measurements of our sol−gel samples are consistent with the development of less polymerized silicon species when high field strength codopants are present. Selected results are included in Figure 7 which shows Raman spectra for samples codoped with Sr^{2+} and Lu^{3+}. The Sr^{2+} codoped sample represents the low field strength limit of the samples of this study. The principle Raman features in the Sr^{2+} codoped sample (Figure 7a) and their assignments[53,54,58−61] are ~1060 cm^{-1} (Q^3), ~975 cm^{-1} (Q^2), ~800 cm^{-1} (motion of Si in a tetrahedral oxygen cage), ~600 cm^{-1} (SiO_2 defect), and <500 cm^{-1} (Si−O−Si modes). When Lu^{3+} replaces Sr^{2+} as the codopant (Figure 7b), a noticeable increase in the Q^2 feature relative to the Q^3 feature and the development of a new Q^1 feature near 900 cm^{-1} are observed. The Q^1 feature becomes more pronounced when Lu^{3+}:Eu^{3+} molar ratio is increased to 9:1 (Figure 7c).

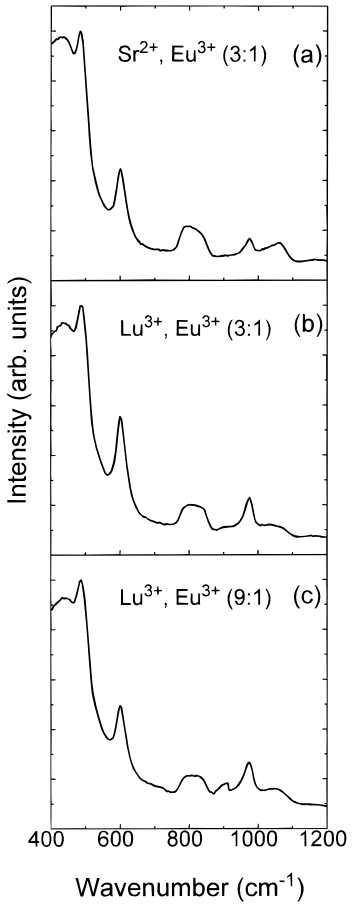

Figure 7. Raman spectra of 1 wt % Eu_2O_3 sol−gel silica codoped with (a) 3:1 molar ratio of Sr^{2+}:Eu^{3+}, (b) 3:1 molar ratio of Lu^{3+}:Eu^{3+}, and (c) 9:1 molar ratio of Lu^{3+}:Eu^{3+}. The spectra are normalized to the maximum intensity feature.

The simultaneous occurrence of less polymerized Q^n species and larger crystal field splittings suggests that the strong crystal field Eu^{3+} bonding sites that develop in the presence of high field strength codopants are likely to include nonbridging oxygens from less polymerized Q^n species. This suggestion implies that the strong crystal field bonding sites occur at the interface of the modifier-rich and modifier-deficient regions of the glass and that interactions between Eu^{3+} and less polymerized Q^n species play an important role in inhibiting the formation of clusters.

Luminescence Decay Curves. Luminescence lifetimes can in principle assist in recognizing the presence of clustered metal ions because clustering leads to fast energy transfer, luminescence quenching, and lifetime shortening. The lifetime of Nd^{3+}, for example, has frequently been used as a measure of the dispersion of Nd^{3+} ions, with longer lifetimes corresponding to better dispersed, less clustered ions.[19] The presence of water, hydroxyl groups, and silanol groups complicate the interpretation of lifetimes in sol−gel systems because these species lead to enhanced nonradiative decay of luminescent ions through hydroxyl quenching.

Even with this caveat in mind, the lifetime data in Table 1 are supportive of an inhibition of clustering by the codopants. The selective excitation luminescence

(55) Hölsä, J.; Porcher, P. *J. Chem. Phys.* **1982**, *76*, 2790.
(56) Piriou, B.; Fahmi, D.; Dexpert-Ghys, J.; Taitai, A.; Lacout, J. L. *J. Lumin.* **1987**, *39*, 97.
(57) Cormier, G.; Capobianco, J. A.; Morrison, C. A.; Monteil, A. *Phys. Rev. B* **1993**, *48*, 16290.
(58) Brawer, S. A.; White, W. B. *J. Chem. Phys.* **1975**, *63*, 2421.
(59) Matson, D. W.; Sharma, S. K.; Philpotts, J. A. *J. Non-Cryst. Solids* **1983**, *58*, 323.
(60) Brawer, S. A.; White, W. B. *J. Non-Cryst. Solids* **1977**, *23*, 261.
(61) McMillan, P. *Am. Miner.* **1984**, *69*, 645.

data indicate that the sample doped only with Eu^{3+} exhibits the greatest extent of clustering. This sample has a lifetime of ~1.23 ms. Much longer lifetimes are observed in the presence of the codopants. The lifetime of the Sr^{2+} codoped sample is longer than is typically found in melt-prepared Eu^{3+}-doped silicate glasses.[46] The decrease in lifetime observed when going from the divalent Sr^{2+} codopant to any of the trivalent codopants is likely due to increased hydroxyl quenching. Higher field strength cations will lead to greater hydroxyl retention than low field strength cations. The relatively constant lifetime observed from La^{3+} through Sc^{3+} probably reflects a balance between the increased hydroxyl retention and better cluster inhibition properties of the codopant as the field strength increases. The decreased lifetime of the Ga^{3+} codoped sample indicates that beyond Sc^{3+}, the hydroxyl quenching effect dominates. This observation is consistent with the leveling of the cluster inhibition effect observed with increasing codopant field strength in the FLN studies. In previous work using Al^{3+} as a codopant in TEOS based glasses,[43] an even shorter lifetime was observed (~0.95 ms).

Conclusions

The ability of cation codopants to inhibit the clustering of Eu^{3+} in sol−gel silica has been considered using fluorescence line-narrowing spectroscopy and Raman scattering measurements. The results indicate a correlation between the ability of a codopant to inhibit Eu^{3+} clustering and the field strength of the codopant. The addition of a high field strength codopant leads to the formation of strong crystal field bonding sites for Eu^{3+}. The characteristics of these sites include a more ionic bonding environment for Eu^{3+}, the presence of bridging oxygen bonding between Eu^{3+} and the codopant, and stronger interactions with nonbridging oxygens associated with less polymerized network-forming species.

The results are consistent with a modified random network model of glass structure which includes crystal chemistry considerations. In samples doped only with Eu^{3+}, the Eu^{3+} ions form local clusters randomly distributed in the glass. Our results suggest that cation codopants penetrate these clusters and interdisperse with Eu^{3+}. This effect leads to larger Eu^{3+}−Eu^{3+} separations and better isolation of Eu^{3+} ions. The effect is more pronounced for higher field strength codopants because they more effectively disrupt the glass network to produce the less polymerized Q^n species which interact more strongly with Eu^{3+}.

The study indicates that the state of aggregation of a targeted dopant ion in sol−gel glasses can be controlled to a certain extent by the concentration and field strength of cation codopants. Chemical modifications that promote stronger interactions between metal-ion dopants and glass-forming regions are expected to lead to more uniform dopant dispersion in sol−gel glasses.

Acknowledgment. The authors gratefully acknowledge financial support from the National Science Foundation—Division of Earth Sciences and the University of Wisconsin Graduate School. V.C.C. acknowledges financial support from the Brazilian National Council of Research, CNPq.

CM9504910